THE JOURNAL OF PHYSICAL CHEMISTRY A

Article

pubs.acs.org/JPCA

Spectroscopic Investigation of Photoinduced Charge-Transfer Processes in FTO/TiO_2/N719 Photoanodes with and without Covalent Attachment through Silane-Based Linkers

Bill Pandit,[†,‡,∥] Tulashi Luitel,[†,‡,∥] Dustin R. Cummins,[§,‡] Arjun K. Thapa,[‡] Thad Druffel,[‡] Frank Zamborini,[†,‡] and Jinjun Liu*[,†,‡]

[†]Department of Chemistry, University of Louisville, Louisville, Kentucky 40292, United States

[‡]Conn Center for Renewable Energy Research, University of Louisville, Louisville, Kentucky, 40292, United States

[§]Department of Chemical Engineering, University of Louisville, Louisville, Kentucky 40292, United States

ABSTRACT: Understanding electron-transfer (ET) processes in dye-sensitized solar cells (DSSCs) is crucial to improving their device performance. Recently, covalent attachment of dye molecules to mesoporous semiconductor nanoparticle films via molecular linkers has been employed to increase the stability of DSSC photoanodes. The power conversion efficiency (PCE) of these DSSCs, however, is lower than DSSCs with conventional unmodified photoanodes in this study. Ultrafast transient absorption pump−probe spectroscopy (TAPPS) has been used to study the electron injection process from N719 dye molecules to TiO_2 nanoparticles (NPs) in DSSC photoanodes with and without the presence of two silane-based linker molecules: 3-aminopropyltriethoxysilane (APTES) and *p*-aminophenyltrimethoxysilane (APhS). Ultrafast biphasic electron injection kinetics were observed in all three photoanodes using a 530 nm pump wavelength and 860 nm probe wavelength. Both the slow and fast decay components, attributed to electron injection from singlet and triplet excited states, respectively, of the N719 dye to the TiO_2 conduction band, are hindered by the molecular linkers. The hindering effect is less significant with the APhS linker than the APTES linker and is more significant for the singlet-state channel than the triplet-state one. Electron injection from the vibrationally excited states is less affected by the linkers. The spectroscopic results are interpreted on the basis of the standard ET theory and can be used to guide selection of molecular linkers for DSSCs with better device performance. Other factors that affect the efficiency and stability of the DSSCs are also discussed. The relatively lower PCE of the covalently attached photoanodes is attributed to the multilayer and aggregation of the dye molecules as well as the linkers.

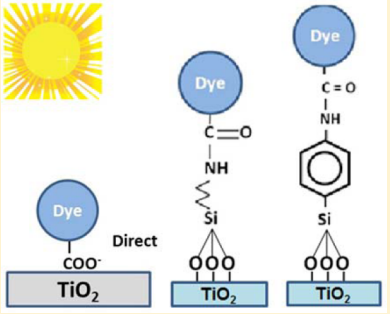

INTRODUCTION

The dye-sensitized solar cell (DSSC) has become one of the most promising photovoltaic devices because of its low cost and relatively high power conversion efficiency (PCE).[1−5] DSSCs consist of a photoanode, with dye-adsorbed nanocrystalline semiconductor film, e.g., TiO_2, on a highly transparent and conductive substrate, such as fluorine-doped tin oxide (FTO); a redox electrolyte, usually iodide/triiodide; and a cathode made of a conductive sheet, such as platinum nanoparticles, on a (typically FTO) substrate. Much research has been done to increase the PCE of DSSCs. PCE close to 12% has been reported for DSSCs based on ruthenium complex dyes on TiO_2 nanoparticle (NP) films; slightly higher PCE has been achieved using porphyrin-based sensitizers.[6−8] Fewer studies, however, have been carried out to optimize other factors of the device performance of DSSCs, especially their stability. Upon air exposure, a traditional DSSC photoanode loses its efficiency completely after 20 days.[9,10] The efficiency is also affected by exposure to heat, water, acids, UV illumination, and desorption of the dye molecules from the semiconductor nanoparticles.[11,12] Sealing the DSSCs improves their stability but cannot completely prevent long-term degradation.[13]

Performance of DSSCs can be improved by modification of photoanodes. Both premodification[14] and postmodification[15] by 3-aminopropyltriethoxysilane (APTES) have been studied previously to increase the efficiency of DSSCs using Ru-based dye. Recently, Luitel et al.[9] used APTES as molecular linkers to covalently attach N719 dye molecules to TiO_2 films and observed a dramatic improvement in photoanode stability. The linker molecule is covalently attached to the N719 dye molecule via an amide bond and anchored to the TiO_2 nanoparticle by its silane group. For DSSCs with the APTES-attached photoanodes, the PCE remains stable after air exposure for more than 60 days.[9] However, the PCE of the DSSCs with covalently attached photoanodes is reduced compared to DSSCs with conventional unmodified photoanodes. A 50% drop in PCE (from ∼6% to ∼3%) was observed for DSSCs with APTES-attached photoanodes when the soaking time in dye solution was the same.[9]

Special Issue: Terry A. Miller Festschrift

Received: July 22, 2013
Revised: October 15, 2013
Published: October 16, 2013

The PCE of solar cells strongly depends on photoinduced dynamics, which can be investigated by time-domain laser spectroscopy. Electron injection from the excited states of dye molecules to the conduction band (CB) of mesoporous semiconductor films usually occurs on a time scale of <100 fs to hundreds of picoseconds[16−21] and consists of several competing processes. The back electron transfer occurs in the microsecond time range.[22−26] To unravel the effect of covalent attachment using molecular linkers on the PCE of DSSCs, in the present work, the electron injection process in the covalently attached photoanode with FTO/TiO_2/APTES/N719 configuration was studied by ultrafast transient absorption pump−probe spectroscopy (TAPPS). To examine the effect of different linkers on the electron injection process an aromatic linker, *p*-aminophenyltrimethoxysilane (APhS), was also investigated and compared to APTES. The conventional unmodified photoanode with the FTO/TiO_2/N719 configuration as well as the N719 solution was also studied for comparison. In addition, attenuated total reflectance-Fourier transform infrared (ATR-FTIR) and steady-state UV/visible absorption spectra of the photoanodes and the solution were obtained to help understand the time-resolved investigation. The experimentally observed spectra are used to explain the change in PCEs.

The comparative study of photoinduced electron-transfer (ET) processes in the presence of molecular linkers is also of significant fundamental interest. ET in bulk solid/liquid interfaces is generally described by the theoretical model first developed by Marcus, Gerischer, and Levich in the 1960s.[27−29] The ET rate depends on both the relative energetics and the electronic coupling of the donor and the acceptor: the dye molecule−semiconductor nanoparticle junction can be regarded as a donor−bridge−acceptor (D−B−A) complex with a dye sensitizer (electron donor) attached to the semiconductor NP film surface (electron acceptor) through a molecular spacer and an anchoring group (bridge). The electronic coupling is determined by both the spacer and the anchoring group. Previously, the dependence of the electron injection rate on the bridge length has been studied using molecules with variable spacer units, e.g., methylene groups[30] or *p*-phenylene groups.[31,32] In the present work, the electron donor and acceptor are connected by a linker molecule that is different from the dye sensitizer. It therefore provides a unique case to study the effect of bridges on ET dynamics.

EXPERIMENTAL SECTION

Chemicals and Materials. Two types of TiO_2 nanoparticles (NPs) were employed in this work. TiO_2 paste DSL 18 NR-T (18 nm) and WREO-2 (150−250 nm) were purchased from Dyesol. *cis*-Diisothiocyanatobis(2,2′-bipyridyl-4,4′-dicarboxylato)Ru(II) bis(tetrabutylammonium) (N719) was purchased from Solaronix. 3-Aminopropyltriethoxysilane (APTES), *N*′-dicyclocarbodiimide (DCC), 4-dimethylaminopyridine (DMAP), acetonitrile, *tert*-butanol, ethyl cellulose, and terpineol were purchased from Sigma-Aldrich. *p*-Aminophenyltrimethoxysilane (APhS) was purchased from Gelest. Fluorine doped tin oxide (F:SnO_2, FTO) glass slides (specific contact resistance = 8−10 Ω/cm^2) were purchased from Hartford Glass Corp. 2-Propanol (IPA) and ethanol (99.99%), titanium tetrachloride ($TiCl_4$), dimethyl sulfoxide, and acetone were purchased from VWR. Nanopure water with resistivity >18 MΩ/cm was used for all aqueous solutions.

Preparation of TiO_2 Film. FTO slides were cleaned by sonicating in acetone, EtOH, and IPA for 10 min each and dried under a N_2 stream for 30 s. The cleaned FTO slides were then soaked in a 40 mM aqueous solution of $TiCl_4$ and heated in a water bath at 70 °C for 30 min. A 0.25 cm^2 exposed area was made on the $TiCl_4$ treated FTO slides by using Scotch tape. A small amount of DSL (18 nm) TiO_2 paste was kept on one edge and spread by a sharp blade on the exposed part to obtain an active layer with uniform thickness. The deposited paste was sintered at 500 °C for 1 h in a 1300 BL Barnstead Thermolyne furnace. A second scattering layer (WREO-2, 150−250 nm) was deposited with the same method on the FTO slides and sintered at 500 °C for 1 h. Finally, the film containing two layers of TiO_2 pastes (active layer and scattering layers) was treated with 40 mM $TiCl_4$ in water at 70 °C for 30 min. This is referred to as the FTO/TiO_2 electrode. Note that for all TAPPS measurements, the scattering layer was not used.

Functionalization of TiO_2 Film. *Chemical Modification with APTES.* The TiO_2 film on FTO (FTO/TiO_2 electrode) was placed inside a 43 mM solution of APTES in IPA with 0.1% of nanopure water.[33] The solution was placed in a water bath at 70 °C for 30 min. The electrode was rinsed thoroughly with IPA and dried under a N_2 stream for 1 min. This is referred to as the FTO/TiO_2/APTES electrode.

Chemical Modification with APhS. The FTO/TiO_2 electrode was placed inside a solution containing 20 mL of DMSO and 2 g of APhS and heated at 130 °C for 3 h.[34] The electrode was rinsed thoroughly with EtOH and dried under a N_2 stream for 1 min. This is referred to as the FTO/TiO_2/APhS electrode.

Previously, it was reported that, when SiO_2 was used as substrate, the primary-amine coverage using 3-aminopropyltrimethoxysilane (APS) and APhS could reach as high as 88.6% and 100%, respectively.[35] Similar coverage of APTES and APhS on TiO_2 is expected.

Dye Sensitization of TiO_2 Film and Covalent Attachment. Sensitization of the FTO/TiO_2 electrodes was achieved by immersing them into a 0.3 mM solution of N719 dye in a 1:1 mixture of acetonitrile and *tert*-butanol.[36] The electrodes were soaked in a dye solution for 24 h. To prepare photoanodes with covalently attached dye sensitizer, the functionalized FTO/TiO_2/APTES and FTO/TiO_2/APhS electrodes were soaked in 0.3 mM dye solution containing 20 mM of DMAP and 20 mM of DCC in 10 mL of methylene chloride.[33] This makes the covalent attachment of dye molecules with APTES and APhS linkers via amide bonds. They are referred to as FTO/TiO_2/APTES/N719 and FTO/TiO_2/APhS/N719 photoanodes. Interactions between dye and FTO/TiO_2, FTO/TiO_2/APTES, and FTO/TiO_2/APhS are depicted in Figure 1a−c. Given their four carboxyl/carboxylic acid groups, N719 dye molecules may attach to the TiO_2 nanoparticles via multiple linker molecules. Parts a−c of Figure 1 show only the single attachment situation. An accurate measurement of the percentages of the singly and multiattached dye molecules was not attempted.

Spectroscopic Characterization. To determine how APTES and APhS interact with the N719 dye, spectroscopic studies were carried out to characterize the photoanodes, including attenuated total reflectance-Fourier transform infrared (ATR-FTIR) and UV/visible absorption spectroscopy. In ATR-FTIR measurement, photoanodes were placed onto the ZnSe crystal in the spectrometer (Perkin-Elmer, Spectrum 100) with the dye layer facing the crystal and held at a pressure of 80

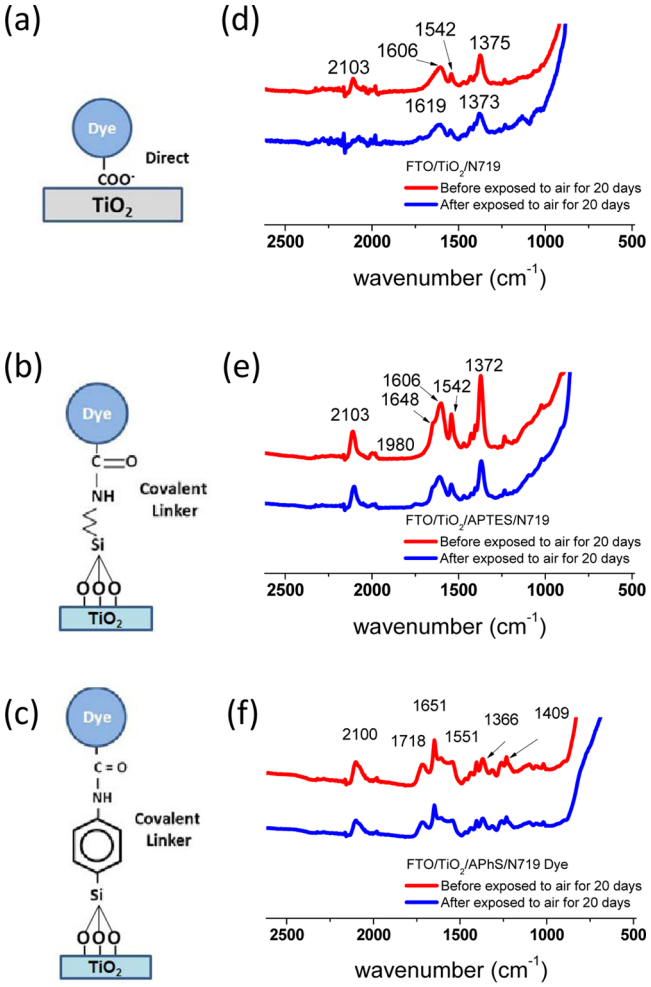

Figure 1. Schemes of the N719 dye attached to TiO_2 films by (a) the conventional direct method, (b) a covalent APTES linker, and (c) a covalent aromatic APhS linker, and the corresponding ATR-FTIR spectra of the photoanodes measured before (red lines) and after (blue lines) exposure to air for 20 days (d–f). In (a)–(c), only the single attachment situation is shown (see text for more details). Spectra are offset for clarification. Assignment of ATR-FTIR peaks are discussed in refs 9 and 37. Note the loss in the CN stretch peak at 2103 cm^{-1} in the conventional photoanode spectra after air exposure. Spectra in (d) and (e) are adapted from ref 9.

psi. Scans were taken from 400 to 4000 cm^{-1} with 20 averages and a resolution of 4 cm^{-1}. To reveal the mechanism for stabilization of photoanodes by covalent linkers, spectra before and after air exposure for 20 days were obtained.

UV/visible absorption spectra of the covalently attached photoanodes were obtained with a Varian Cary Win UV–vis spectrophotometer. Absorption spectra of N719 in (1:1) ACN and *tert*-butanol solution and conventional FTO/TiO_2/N719 photoanodes were also recorded for comparison.

Ultrafast Transient Absorption Pump–Probe Spectroscopy (TAPPS). Ultrafast transient absorption pump–probe spectroscopy (TAPPS) measurements were performed on N719 in (1:1) ACN and *tert*-butanol solution, on conventional FTO/TiO_2/N719 photoanodes, and on covalently attached FTO/TiO_2/APTES/N719 and FTO/TiO_2/APhS/N719 photoanodes. The TAPPS system uses a Clark-MXR CPA Ti:sapphire ultrafast laser (wavelength = 775 nm, pulse duration $\lesssim$150 fs, pulse energy ~1 mJ at 1 kHz repetition rate). Output from the CPA is split and used to pump two noncollinear optical parametric amplifiers (NOPAs), which in total are able to cover a wavelength region 450–1600 nm. Part of the CPA output is also separated to pump a 3 mm thick sapphire plate to generate supercontinuum white-light (420–1600 nm). Output from the first NOPA at 530 nm wavelength was pulse-compressed to ~30 ± 5 fs determined by an autocorrelation measurement. It was used as the pump light source. The pulse energy of the pump light is attenuated to below 0.2 μJ to avoid unwanted multiphoton excitation and thermal degradation of the samples. Both the white-light and the 860 nm output from the second NOPA were used as the probe light. In all measurements reported here, polarizations of the pump and probe beams are parallel. The probe beam is focused onto the sample while the pump beam is slightly defocused to ensure the coverage of the probe beam. After the sample, the pump beam is blocked by a notch filter. When the 860 nm probe beam was used, its transmission signal was detected with a Si photodiode (Thorlabs DET10A) and amplified by a lock-in amplifier (SRS SR810), whereas with the white-light probe beam, the transmission is dispersed by a curved grating and detected by a linear array CMOS detector in the wavelength range 430–730 nm. The time delay between pump and probe pulses (Δt) is variable between 0 and 1.5 ns by moving a retroreflector on a computer-controlled translation stage that reflects the pump beam. An optical chopper revolving at 500 Hz, half the repetition rate of the femtosecond laser, is used to modulate the pump beam and the TAPP signal is recorded as the change in optical density (ΔOD) with pump beam blocked and unblocked:

$$\Delta \mathrm{OD}(\Delta t) = -\log\left[\frac{I^*(\Delta t)}{I_0}\right] \quad (1)$$

where I_0 and I^* are the probe beam transmission with the preceding pump beam blocked and unblocked, respectively. Time zero was determined by the transient absorption signal of R6G dye solution, and the group velocity dispersion was corrected. The TAPPS system is controlled by a LabVIEW (National Instruments) program.

RESULTS

ATR-FTIR Spectra. ATR-FTIR spectra of the photoanodes with and without covalent attachment before and after air exposure are compared in Figure 1d–f. The most remarkable change in the spectrum of the conventional photoanode (Figure 1d) is the CN stretch from the two SCN ligands of the N719 dye molecule at 2103 cm^{-1}. It almost completely disappeared after 20 days of air exposure. On the contrary, although decreased, it remained strong in the spectra of FTO/TiO_2/APTES/N719 (Figure 1e) and FTO/TiO_2/APhS/N719 (Figure 1f) photoanodes. Such observation suggests that the improvement in stability of the covalently attached photoanodes is because the linker molecules provide an environment that protects the SCN ligands and retains the photoelectrochemical properties of the dye. Detailed analysis of the spectra and assignment of other IR peaks can be found elsewhere.[9,37]

Steady-State UV/Visible Absorption Spectra. Steady-state absorption spectra of N719 dye in solution and adsorbed on TiO_2 film with and without covalent linkers (APTES and APhS) are shown in Figure 2. In the spectrum of N719 in (1:1) ACN and *tert*-butanol solution (Figure 2a), two absorption

dx.doi.org/10.1021/jp407270j | J. Phys. Chem. A 2013, 117, 13513–13523

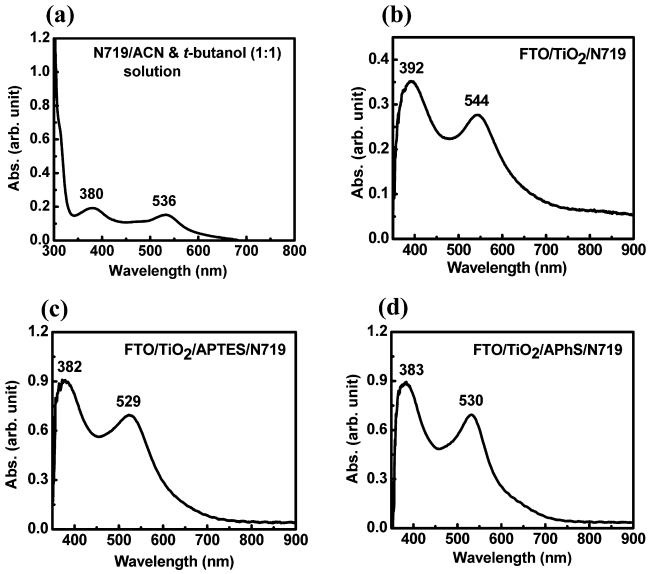

Figure 2. Steady-state UV/visible absorption spectra of (a) N719 dye/ACN and *tert*-butanol (1:1) solution and (b) FTO/TiO_2/N719, (c) FTO/TiO_2/APTES/N719, and (d) FTO/TiO_2/APhS/N719 photoanodes.

maxima are observed at 380 and 536 nm, which are assigned as metal-to-ligand charge-transfer (MLCT) transitions (4d−π*).[38] The long wavelength tail (up to 750 nm) was attributed to transition to the luminescent $[Ru^{III}(bpy)_2bpy^-]^{2+}$ excited state.[39] In the spectrum of the conventional photoanode, in which the N719 dye is directly adsorbed on TiO_2 NPs (Figure 2b), the two absorption bands at 380 and 536 nm are red-shifted by 12 and 8 nm, respectively, as compared to absorptions of the N719 dye solution. Previously the red shift was attributed to either the aggregation of dye molecules on the TiO_2 surface[40,41] or protonation equilibria caused by Ti^{4+} as the dye interacts with TiO_2.[42] The red shift effect is altered by the linker molecules. Parts c and d of Figure 2 show the absorption spectra of N719 dye covalently attached to TiO_2 NPs by APTES and APhS, respectively. The insertion of APTES between TiO_2 and the N719 dye causes a blue shift of the absorption peaks compared to the case of the conventional FTO/TiO_2/N719 photoanode. A blue shift with essentially the same magnitude is observed in the UV/visible spectrum of the FTO/TiO_2/APhS/N719 photoanode. The observed blue shifts in FTO/TiO_2/APTES/N719 and FTO/TiO_2/APhS/N719 photoanodes suggest that the red shift in the absorption spectrum of the N719 dye upon adsorption on TiO_2 NPs is mainly due to the interaction between the dye sensitizer and the semiconductor NPs, which can be altered by different choice of the molecular linker, and hence supports the aforementioned protonation-equilibria interpretation. Furthermore, a significant increase in absorption was observed for the covalently attached photoanodes compared to the conventional one, suggesting multilayer and aggregation of dye molecules.

TAPP Spectra. The TAPPS experiment directly measures the electron injection dynamics in the photoanodes by varying the time delay between the pump and probe pulses. It also reveals details of the electron injection process by the probe-wavelength dependence. In the present work, 530 nm pump source was used to excite N719 to its MLCT band (Figure 2). Two probe light sources were used: single-wavelength 860 nm

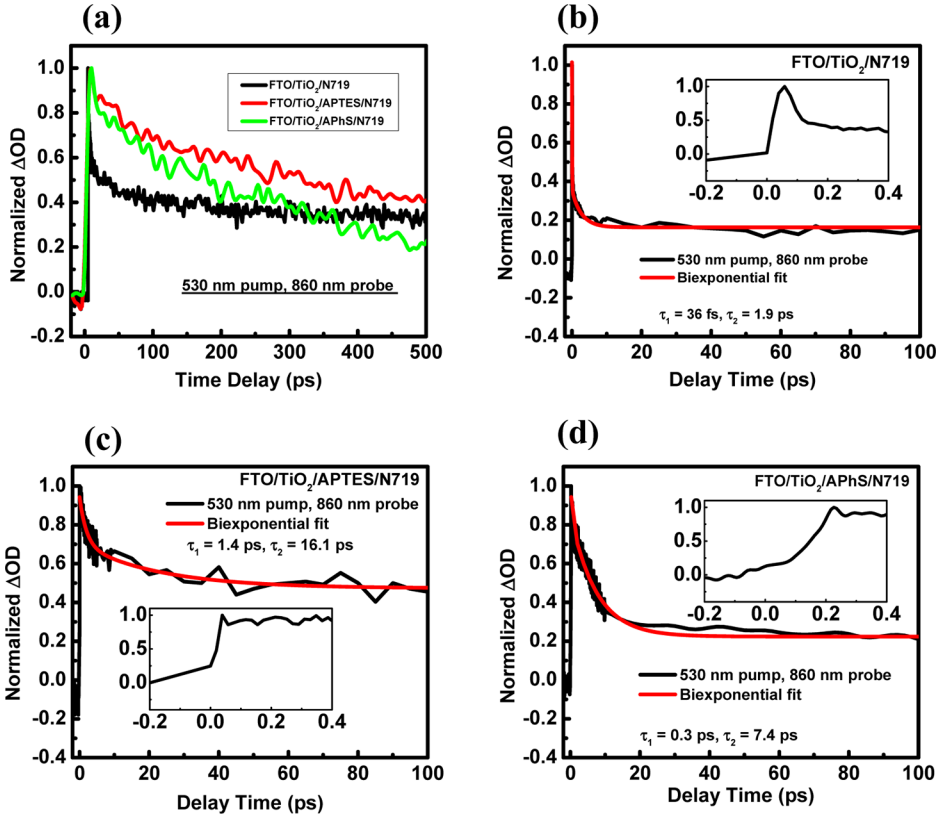

Figure 3. (a) Normalized transient absorption kinetics observed with the 530 nm pump wavelength and 860 nm probe wavelength of FTO/TiO_2/N719, FTO/TiO_2/APTES/N719, and FTO/TiO_2/APhS/N719 photoanodes. (b)−(d) illustrate the kinetics up to 100 ps and the biexponential fits.

dx.doi.org/10.1021/jp407270j | J. Phys. Chem. A 2013, 117, 13513−13523

Table 1. Fit Parameters for TAPPS Kinetics[a]

probe wavelength (nm)	photoanodes	A_0 (au)	A_1 (au)	τ_1 (ps)	A_2 (au)	τ_2 (ps)
860	FTO/TiO_2/N719	0.163 ± 0.004	0.661 ± 0.015	0.036 ± 0.002	0.191 ± 0.005	1.928 ± 0.111
	FTO/TiO_2/APTES/N719	0.473 ± 0.019	0.242 ± 0.026	1.364 ± 0.230	0.229 ± 0.023	16.071 ± 6.136
	FTO/TiO_2/APhS/N719	0.224 ± 0.006	0.290 ± 0.077	0.278 ± 0.056	0.628 ± 0.006	7.419 ± 0.164
690	FTO/TiO_2/N719	0.263 ± 0.009	0.765 ± 0.007	2.317 ± 0.602		
	FTO/TiO_2/APTES/N719	0.607 ± 0.015	0.338 ± 0.013	4.424 ± 0.232		
	FTO/TiO_2/APhS/N719	0.335 ± 0.054	0.642 ± 0.047	3.267 ± 0.423		

[a]The fit curves as well as experimentally measured kinetics are illustrated and compared in Figure 3 (for 860 nm probe wavelength) and Figure 7 (for 690 nm probe wavelength).

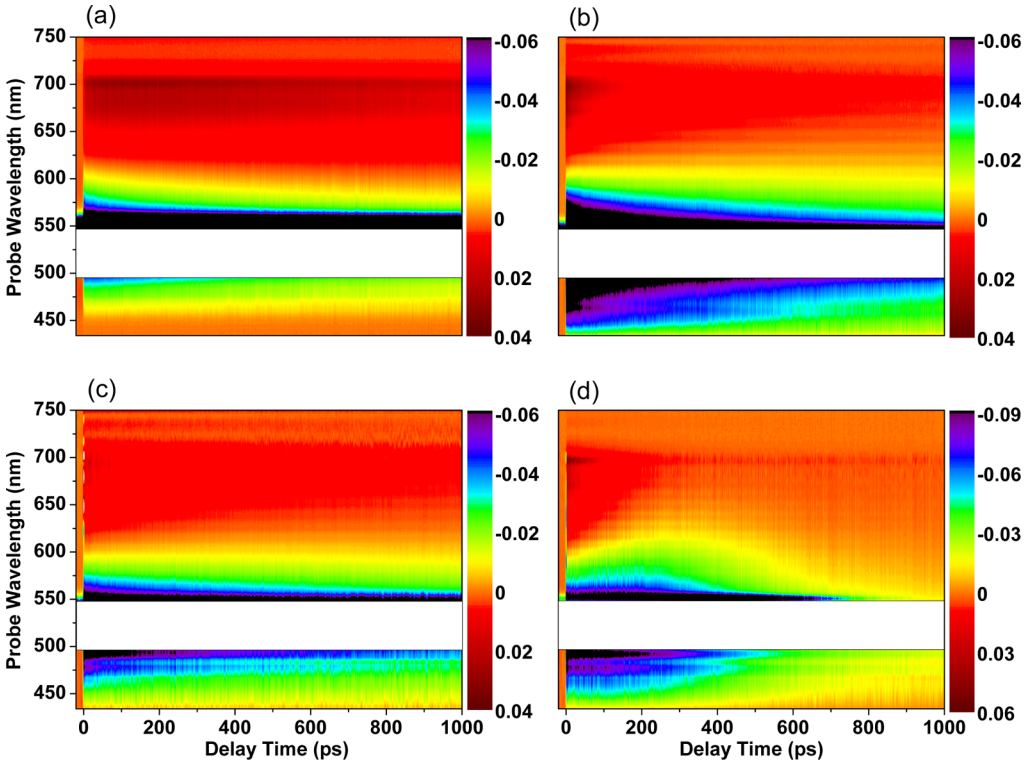

Figure 4. Transient absorption 2D time–wavelength contour plots of (a) N719 dye/ACN and *tert*-butanol (1:1) solution and (b) FTO/TiO_2/N719, (c) FTO/TiO_2/APTES/N719, and (d) FTO/TiO_2/APhS/N719 photoanodes.

output from a NOPA and supercontinuum white light. Due to its relative simplicity, the result with the 860 nm probe wavelength is presented first.

TAPP Spectra with 860 nm Probe Beam. Figure 3a shows transient absorption kinetics of FTO/TiO_2/N719, FTO/TiO_2/APTES/N719, and FTO/TiO_2/APhS/N719 photoanodes up to 500 ps with an excitation wavelength of 530 nm and a probe wavelength of 860 nm. The decay curves are biphasic and can be fit to a biexponential function as follows:

$$\Delta OD(\Delta t) = A_0 + A_1 e^{-\Delta t/\tau_1} + A_2 e^{-\Delta t/\tau_2} \quad (2)$$

with $\tau_1 < \tau_2$. The fit parameters for the three photoanodes are listed in Table 1. It has been generally accepted that the faster and slower decay components correspond to electron injection from the singlet and triplet MLCT states, respectively.[6,43−45] Previously, decay dynamics in shorter than 10 fs were observed by ultrafast time-gate fluorescence spectroscopy[45] and attributed to a nonergodic electron injection process from nonequilibrated singlet excited states of N719 to TiO_2. Limited by the time resolution of the probe source (~60 fs), such a fast process was not observed in the present experiment.

The time scales (τ_1 and τ_2) are significantly different among the three photoanodes. Upon insertion of APTES linker, the time scale for the electron injection process from the singlet states of N719 to the conduction band of TiO_2 (τ_1) increases from 36 fs to 1.4 ps, whereas that from the triplet states (τ_2) increases from 1.9 to 16.1 ps. The increment in decay time scale is less significant when the APhS linker is used: to τ_1 = 0.3 ps and τ_2 = 7.4 ps. Note that the fit values of the time scales of the fast decay component (τ_1), especially for the conventional photoanode, are comparable to the pulse duration and the instrument response function (IRF) of the TAPPS system. The fit values of τ_1 are therefore not accurate measures of the electron injection rates but should be regarded as only semiquantitative estimates. Comparison among the three photoanodes, however, demonstrates the effect of the molecular linkers in hindering the electron injection processes.

A rise time of ~50 fs prior to the decay has been observed in TAPP spectra of the FTO/TiO_2/N719 photoanode (inset of Figure 3b). Such a rise time is dominated by IRF but also contains contributions from intermolecular vibrational redistribution (IVR) and internal conversion (IC) in both the singlet and triplet excited-state N719 molecules, which

dx.doi.org/10.1021/jp407270j | J. Phys. Chem. A 2013, 117, 13513−13523

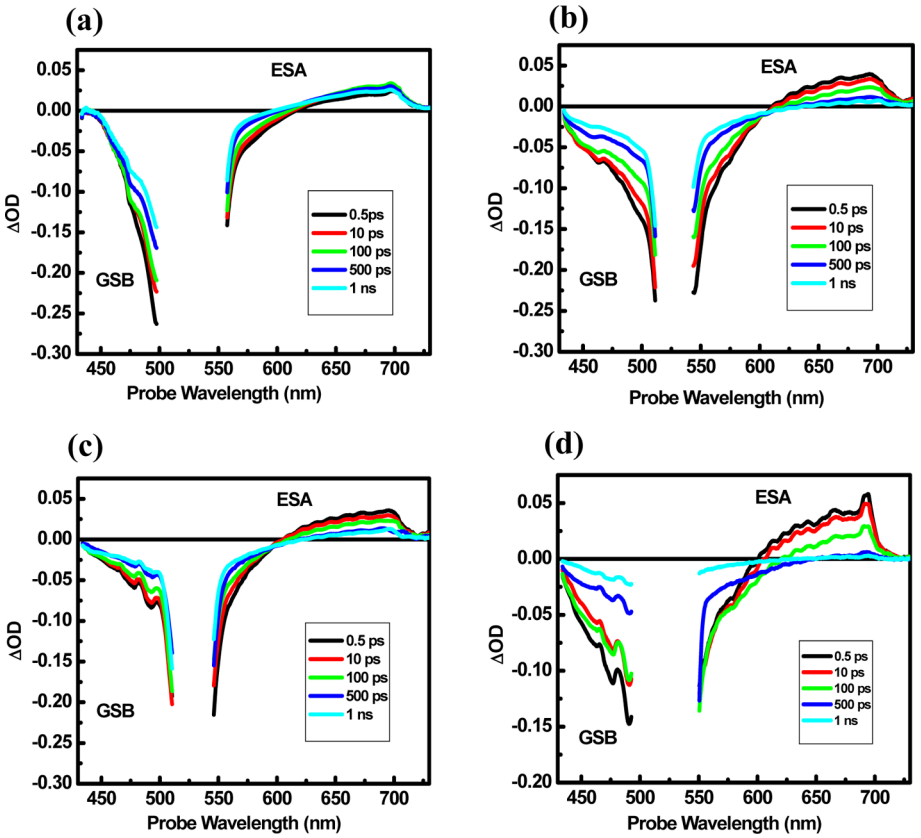

Figure 5. Transient absorption spectra at Δt = 0.5 ps, 10 ps, 100 ps, 500 ps, and 1 ns of (a) N719 dye/ACN *tert*-butanol (1:1) solution and (b) FTO/TiO_2/N719, (c) FTO/TiO_2/APTES/N719, and (d) FTO/TiO_2/APhS/N719 photoanodes. Two broad spectral regions, ground-state bleach (GSB) and excited-state absorption (ESA), are indicated.

equilibrate the molecules. A similar rise time was observed for the FTO/TiO_2/APTES/N719 photoanode (inset of Figure 3c), whereas it is prolonged when APhS is used as the linker (inset of Figure 3d) probably due to the effect of the aromatic ring on the IVR and IC dynamics. Quantitative analysis, however, was not attempted due to the limited time resolution and instrumental response.

It is worth noting that an offset, A_0 in eq 2, was introduced in the biexponential fitting of all three TAPP decay dynamics. Such a long-lasting signal can only be attributed to triplet state dye molecules that are not subject to ET processes due to poor coupling. Previously, a slow component of the observed electron injection process in TiO_2/N719 solar cell was attributed to dye molecules that are loosely attached onto the surface or are present in an aggregated form.[46] Such an offset is therefore evidence of multilayer or aggregates of N719 dye molecules. Because only the first layer of molecular sensitizer undergoes efficient electron injection to TiO_2 NPs, N719 molecules in other layers can stay in triplet states after photoexcitation and the ensuing ISC. The A_0 value is larger for FTO/TiO_2/APTES/N719 and FTO/TiO_2/APhS/N719 photoanodes than the conventional one, which partially explains their relatively lower PCE. It is also consistent with the stronger UV/visible absorption observed for these two phtoanodes. (Compare Figure 2c,d to Figure 2b.)

TAPP Spectra with White-Light Probe. TAPP spectra using white-light as the probe source and detected in the 430−730 nm region are illustrated in Figure 4. The step size of the delay time was relatively large (3 ps) in obtaining the spectra in Figure 4. The time−wavelength plots of all four samples, N719 dye dissolved in 1:1 ACN and *tert*-butanol solvent and FTO/TiO_2/N719, FTO/TiO_2/APTES/N719, and FTO/TiO_2/APhS/N719 photoanodes, show a similar pattern: signals in the wavelength region longer than 600 nm are predominantly positive, whereas those in the shorter wavelength region are predominantly negative. The positive signals are due to excited-state absorption (ESA) and directly related to the formation and relaxation of excited (singlet or triplet) states and oxidized states of the dye molecules after photoexcitation. The negative signals are attributed to the ground-state bleach (GSB). We rule out any major contribution from stimulated emission (SE) to the negative signals on the basis of two facts: (1) The negative signal is roughly symmetric on both sides of the pump wavelength (530 nm). Due to the fast IVR/IC (<10 fs) and ISC (<30 fs) processes,[45] the SE process would contribute mostly in the longer wavelength region and make the spectra asymmetric. (2) No evidence of SE was found in the positive-signal region with wavelength >600 nm except for the N719 solution because the decay kinetics are single-exponential within 10 ps delay time (see below).

From the 2D contour plots, transient absorption spectra in the 430−730 nm range at different delay times (Δt = 0.5 ps, 10 ps, 100 ps, 500 ps, and 1 ns) are extracted and shown in Figure 5. Time evolution of the transient absorption spectrum of the N719 dye solution (Figure 5a) is different in the two wavelength regions longer and shorter than 600 nm. The ESA signal in the >600 nm region builds up completely within ~100 ps after photoexcitation and thereafter decays slowly on a time scale much longer than nanoseconds. In contrast, the GSB signal in the <600 nm region demonstrates a continuous

dx.doi.org/10.1021/jp407270j | J. Phys. Chem. A 2013, 117, 13513−13523

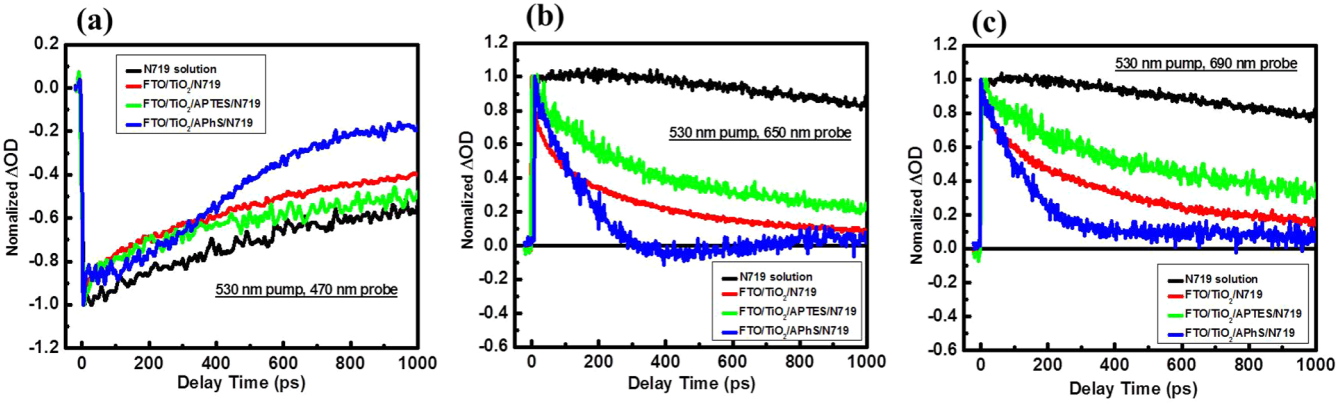

Figure 6. Normalized transient kinetics observed with the 530 nm pump wavelength and (a) 470 nm, (b) 650 nm, and (c) 690 nm probe wavelengths of N719 dye/ACN *tert*-butanol (1:1) solution and FTO/TiO_2/N719, FTO/TiO_2/APTES/N719, and FTO/TiO_2/APhS/N719 photoanodes. The delay time step size is 3 ps.

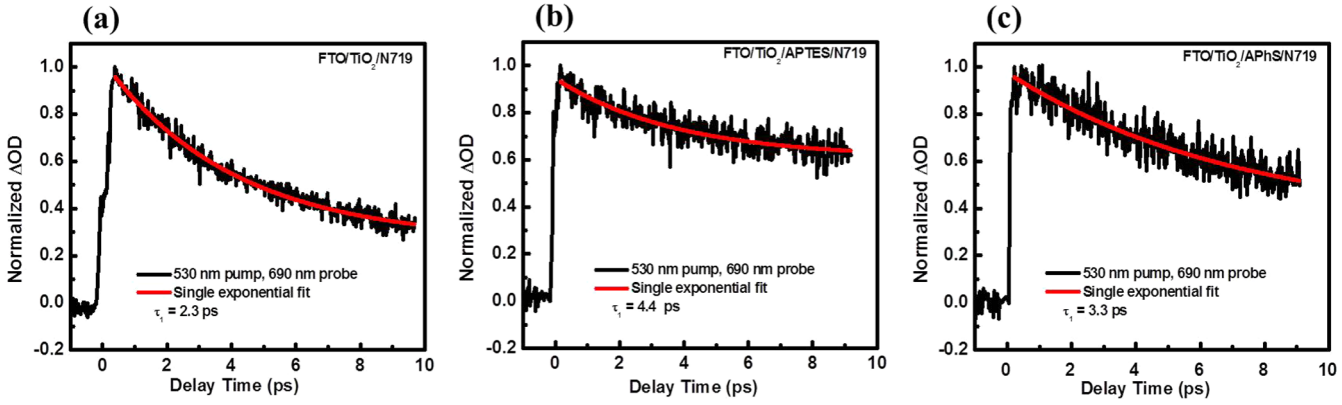

Figure 7. Normalized transient kinetics observed with the 530 nm pump wavelength and 690 nm probe wavelength of (a) FTO/TiO_2/N719, (b) FTO/TiO_2/APTES/N719, and (c) FTO/TiO_2/APhS/N719 photoanodes. The delay time step size is 20 fs.

decrease starting from pump−probe delay time of 0.5 ps due to the ground-state recovery. In the transient absorption spectra of the three photoanodes (Figures 5b−d), similar ground-state recovery dynamics were observed. However, the dynamics of the ESA signals are different from those of the solution. No buildup was observed; instead, one sees the decay of ESA signal immediately after photoexcitation. On the basis of these observations, we conclude that the buildup behavior observed for the positive signal of the N719 solution in the region longer than 600 nm is actually a combined effect of ESA and SE: an SE process with a time scale of ∼100 ps competes with the ESA process, resulting in a reduced positive signal. When attached to TiO_2 NPs, either directly or via molecular linkers, the excited state is depopulated in picoseconds (see below) through electron injection to the TiO_2 NPs. Such a fast electron injection process prevents the SE process, hence the disappearance of the buildup of the ESA signal. The exact mechanism of the SE process is still undetermined but probably involves triplet states given its relatively large time scale. It is unlikely that the negative contribution is due to GSB because excited states of isolated dye molecules in solution are rather long-lived (∼15−50 ns).[47]

Quantitative information on the time scales of ET processes can be derived by examining the transient decay kinetics at particular probe wavelengths, extracted from the 2D time-wavelength contour plots. Parts a−c of Figure 6 show the transient decay kinetics of the four samples at 470, 650, and 690 nm probe wavelengths. The GSB signal of the FTO/TiO_2/APhS/N719 photoanode probed at 470 nm shows the fastest recovery among all four samples ($\tau \sim 500$ ps). The other three samples have similar and longer recovery times ($\tau > 1$ ns). The mechanism that leads to the faster recovery of the ground-state N719 population in the FTO/TiO_2/APhS/N719 photoanode is undetermined but might be due to the aromatic nature of the APhS molecule. It is well-known that inclusion of π-electron systems, i.e., increasing the degree of conjugation, improves the fluorescence quantum efficiency.[48] It is worth noting that although not presented in figures, the transient decay kinetics probed at 570 nm, on the red side of the pump wavelength, are almost identical to the ones probed at 470 nm.

The transient decay kinetics probed at 650 and 690 nm are shown in Figure 6b,c. In N719 dye solution, the relaxation of the excited-state population is slow and is preceded by a buildup process discussed previously. The decay time scale is much longer than the limit of delay time of the TAPPS system (1.5 ns). It suggests that the relaxation corresponding to these probe wavelengths is from the triplet ^{3}MLCT state of the N719 dye, following a fast ISC. In the ESA signal of the three photoanodes, the buildup process is absent and the decay is much faster. It consists of a faster component with ∼50 ps time scale, followed by another relatively slower component with ∼500 ps time scale except for the FTO/TiO_2/APhS/N719 photoanode with 650 nm probe (see below). Both components might be due to various recombination processes but from

dx.doi.org/10.1021/jp407270j | J. Phys. Chem. A 2013, 117, 13513−13523

singlet and triplet states, respectively. Again, the decay is faster in the FTO/TiO_2/APhS/N719 photoanode than the other two.

An interesting feature was observed in the transient decay kinetics of the FTO/TiO_2/APhS/N719 photoanode with 650 nm probe wavelength (Figure 6b). Following the first (and faster) decay component, the ΔOD signal changes its sign from positive to negative at ∼300 ps delay time. It changes back to positive signal after ∼400 ps. Such a sign-changing feature is not observed for the other two photoanodes. It suggests that the observed ΔOD signal is a combination of ESA signal and GSB signal. The negative signal probed at 470 nm is dominated by GSB, whose time scale is determined by ground-state recovery. The positive signal probed at 690 nm is dominated by ESA, the time scale of which is determined by charge recombination. It is reasonable to postulate that combination of these processes causes the complicated decay dynamics in the FTO/TiO_2/APhS/N719 photoanode and the sign-changing. A quantitative explanation cannot be reached without further experimental investigation. We do, however, point out that the transient decay of the FTO/TiO_2/APhS/N719 photoanode probed at 690 nm reaches the turning point between the fast and slow components at ∼400 ps (Figure 6c), when the negative ΔOD signal with 650 nm probe reaches its minimum (Figure 6b). A probe delay of ∼400 ps is clearly a critical time point for change in dominant photoinduced processes.

The delay time step size (3 ps) used to obtain the time-wavelength 2D plots in Figure 4 is too large to detect the ultrafast electron injection from the N719 dye. Decay dynamics in the three photoanodes were therefore monitored in TAPPS in a shorter delay time range (up to 10 ps) with the 690 nm probe wavelength. The step size is 20 fs. The recorded decay dynamics and fit curves are shown in Figure 7. Unlike those with the 860 nm probe wavelength (Figure 3b−d), the decay dynamics with the 690 nm probe wavelength are best fit to a single exponential decay. The time constants are 2.3 ± 0.6 ps for FTO/TiO_2/N719, 4.4 ± 0.2 ps for FTO/TiO_2/APTES/N719, and 3.3 ± 0.4 ps for FTO/TiO_2/APhS/N719 photoanodes (see also Table 1). The time scales are comparable to those of the slower components of the decay dynamics probed at 860 nm and can be attributed to electron injection from the triplet states of N719 molecules to the conduction band of the TiO_2 NPs. The rise time observed in Figure 6a−c therefore corresponds to both the formation and ensuing thermalization of the triplet states. The electron injection rate measured at 690 nm decreased upon insertion of molecular linkers. The magnitude of the decrease, however, is less significant than with 860 nm probe wavelength (see the Discussion). As with the 860 nm probe wavelength, the hindering effect of the APhS linker is weaker than for APTES.

DISCUSSION

For a given pair of electron donor and acceptor, the ET rate is determined by both the relative energetics at the semiconductor/sensitizing dye interface and their electronic coupling. In the present work, the electron injection process was investigated at different wavelengths for photoanodes with and without covalent molecular linkers. The linker molecules affect the electronic coupling whereas different probe wavelengths interrogate ET processes corresponding to different energetics.

The biphasic nature of the TAPP spectra of the conventional FTO/TiO_2/N719 photoanode observed using the 860 nm probe beam within a 100 ps delay time (Figure 3b−d) reveals two ET channels from the N719 molecule to the TiO_2 NP: from the singlet states (^{1}MLCT) and triplet states (^{3}MLCT) of N719. The one order of magnitude difference between time scales for the ET processes from the singlet-state and triplet-state N719 are attributed to two factors:[43] (i) the increase of the density of acceptor states in TiO_2 above the edge of its conduction band, resulting in more energy levels available to ET from the singlet excited-state N719 molecule, and (ii) the different electronic nature of singlet and triplet states in N719, resulting in different electronic couplings between the energy levels of the excited donor molecule and the acceptor semiconductor NP.

When the 690 nm probe wavelength is used, the TAPPS kinetics observed in the FTO/TiO_2/N719 photoanode can be fit to a single exponential decay with a time constant of 2.3 ps. This value is close to the time constants of the slower component in the TAPPS kinetics observed using 860 nm probe wavelength (1.9 ps). The decay is therefore attributed to electron injection from triplet-state N719 molecules as well, but most probably with different energetics. Electron injection from the thermalized triplet states is expected to be slower than that from the vibrationally excited levels of the lowest triplet state and higher-energy triplet states, both of which are generated directly by ISC.[49] This is due to the different density of states in the electron acceptor, which explains the slightly longer time scale with 690 nm probe wavelength.

The insertion of covalently attached linker molecules (APTES and APhS) slows down the electron injection processes in all cases. Based on the Marcus theory of ET, two mechanisms may lead to the hindering effect of the molecular linker. First, the linker increases the spatial displacement between the electron donor and acceptor and hence the longer electron injection time scale. Second, the linker molecule affects the energetics for electron injection. For instance, the reorganization energy caused by the acceptor−donor interaction can be affected by the linker.

Previously, ISC on a time scale of ∼30 fs was reported.[45] It is therefore puzzling that electron injection from singlet states, which occurs at much slower rates, was observed in photoanodes with covalent attachment. To explain such an observation, we note that the measured time scales are for electron injection from the dye molecules to the TiO_2 nanoparticles. It is longer than the time scale of electron transfer from dye molecules to linker molecules in the covalently attached photoanodes that is fast enough to compete with ISC. Indeed, on the basis of the fact that we were able to observe electron injection from singlet states in these photoanodes, we conclude that the time scale of electron transfer from the dye molecules to the linker molecules is similar to that of direct electron injection from dye molecules to TiO_2 NPs in the conventional photoanode. It is the molecular linkers that slow down the overall electron injection processes.

The magnitude of the hindering effect depends on the decay channel, the selection of the linker molecule, and the probe wavelength. For TAPPS kinetics probed at 860 nm, electron injection processes from both the singlet states and the triplet states of the N719 dye molecules are slowed down. For both FTO/TiO_2/APTES/N719 and FTO/TiO_2/APhS/N719 photoanodes, the hindering effect is more significant for the singlet-

state channel than the triplet-state channel. The different magnitudes may be attributed to different densities of accepting states in TiO_2 for the two channels. Another more plausible reason is the influence of vibrational motion of the dye molecule. Due to the fast IC/IVR (<10 fs), the electron injection for the singlet states is predominantly from the thermalized levels, whereas electron injection from the triplet states may have significant contribution from vibrationally excited states that are populated directly by ISC (<30 fs). It is known that molecular vibration can affect the electron injection rate.[49] The two channels are therefore affected by the insertion of the linker molecules differently.

The hindering effect also depends on the choice of molecular linkers. The electron injection rates detected at 860 nm are faster (~0.3 ps from singlet states and ~7.4 ps from triplet states) in the FTO/TiO_2/APhS/N719 photoanode than in the FTO/TiO_2/APTES/N719 photoanode (~1.4 ps from singlet states and ~16.1 ps from triplet states). Both linkers increase the distance between the electron donor (dye sensitizer) and the acceptor (TiO_2). The APhS molecule is slightly shorter than the APTES molecule. Because the effect of linker length on the electron injection rate is exponential, the difference in linker length may lead to a considerable difference in electron injection rate. A quantitative calculation requires the determination of the damping factor, β, for the carbon chains and benzene rings and is hence not attempted here. A more significant difference between the linker molecules that explains the difference in electron injection rate between FTO/TiO_2/APhS/N719 and FTO/TiO_2/APTES/N719 photoanodes is their electronic structure: due to its aromatic nature, the molecular orbitals of APhS are more delocalized than APTES and hence have better overlap with the LUMO of the dye molecule and the conduction band orbitals of the NPs. The more conductive nature of the APhS molecules therefore leads to stronger electronic coupling between the donor and acceptor, and hence faster electron injection.

The hindering effect of the linker molecules probed at 690 nm is much less significant than when the 860 nm is used as the probe wavelength. This suggests that the hindering effect of the molecular linkers is different between different vibrational energy levels within a triplet state and probably also between different triplet states. The slower electron injection process observed with the 860 nm probe is from the excited triplet states formed directly by ISC, whereas that observed with 690 nm, blue-shifted from the ESA peak, corresponds to electron injection from the thermalized and equilibrated triplet-state levels. The difference in decay time constants reflects the important role of molecular vibration in the electron injection processes. Electron injection from vibrationally hot molecules is less vulnerable to the hindering effect of the molecular linkers. This is consistent with the different magnitude in the hindering effect for the two components of the decay kinetics observed using 860 nm probe wavelength.

The measurement of electron injection as well as recombination processes can be affected by many other factors, for instance, the existence of multilayer dye molecules, the aggregation of the dye molecules, and different crystal orientations in the TiO_2 film. On the basis of comparison between the TAPPS kinetics measured at different probe wavelengths and using different linker molecules, we conclude that such manufacturing factors do not affect the observed electron injection processes significantly. They can, however, alter the slower recombination processes. For instance, the FTO/TiO_2/APhS/N719 photoanode shows faster electron recombination (Figure 6). Buildup of the ESA signal due to the electron injection from dye sensitizer to semiconductor NPs has been reported previously[50−52] but was not observed in the present work. It was observed for the N719 solution with 690 nm probe wavelength, which may explain the previously reported buildup in the ESA signal.

CONCLUSIONS

The electron injection processes were monitored in TAPPS spectroscopy. The fast and slow components of the decay kinetics with the 860 nm probe are attributed to electron injection from the thermalized singlet states and the vibrationally excited triplet states, respectively. When a visible white-light probe is used, in the shorter wavelength region, e.g., at 470 nm, the signal is dominated by ground-state bleach, whereas in the longer wavelength region, e.g., at 690 nm, electron injection from thermalized triplet states is detected. In the vicinity of the pump wavelength (530 nm), the signal contains contributions from both processes and is further complicated by stimulated emission.

On the basis of the TAPPS measurements, we propose that the electron injection from the excited states of N719 dye to TiO_2 semiconductor conduction band occurs via two channels: a fast channel (tens of femtoseconds) from the singlet states of N719 and a slow channel (~1−10 ps) from its triplet states. The electron injection process is hindered by linker molecules APTES and APhS that are covalently attached to the N719 dye molecules. The magnitude of the hindering effect depends on both the spin-multiplicity of the excited electronic states of the dye and molecular vibrations. The hindering effect is more significant for singlet excited-state molecules than molecules in triplet states. Electron injection from vibrationally excited triplet-state molecules is less vulnerable to the hindering effect. Electron injection processes in the FTO/TiO_2/APhS/N719 photoanodes are faster than in the FTO/TiO_2/APTES/N719 photoanode because the APhS molecule is more conductive due to its aromaticity. Suitable choice of linker molecules is therefore important in producing DSSCs that have both long stability and high PCE.

The stability of the phtotoanodes is significantly increased upon covalent attachment, attributed to the protective environment provided by the linker molecules to the SCN ligands.[9] Although the molecular linkers slow the electron injection process, it is still orders of magnitude faster than the charge recombination to dye molecules and the electrolyte as well. The relatively slower electron injection rate is therefore not the reason for the observed lower PCE of the FTO/TiO_2/APTES/N719 photoanode compared with the conventional one. The relatively lower PCE of the covalently attached photoanodes is mainly due to the multilayer and aggregation of the dye molecules above the covalently bonded ones in addition to the possible multilayer formation of the linker itself. TAPPS results show that the FTO/TiO_2/APhS/N719 photoanode has better coverage of monolayer dye molecules than the FTO/TiO_2/APTES/N719 photoanode. A higher PCE is therefore expected. Monolayer coverage of linkers on semiconductor metal oxide is necessary for improving PCE of such devices, as shown recently.[9] When the soaking time in dye solution was controlled to avoid multilayers, PCE of the FTO/TiO_2/APTES/N719 photoanode was increased to 6.0 ± 1.0%, very close to that of the conventional one (6.5 ± 0.9%). Modification of the covalently attached photoanodes, for

instance, with gold nanoparticles, can further improve the performance of DSSCs with chemically functionalized photoanodes and will be the subject of future work.

AUTHOR INFORMATION

Corresponding Author

*J. Liu: e-mail, j.liu@louisville.edu.

Author Contributions

‖These authors contributed equally to this work.

Notes

The authors declare no competing financial interest.

ACKNOWLEDGMENTS

The authors gratefully acknowledge the financial support of the Department of Energy via its EPSCoR grant (DE-FG02-07ER46375). B.P. and J.L. acknowledge financial support from the University of Louisville. We thank Dr. Mahendra K. Sunkara for his help in the experiment and fruitful discussion.

REFERENCES

(1) O'Regan, B.; Grätzel, M. A low-cost, high-efficiency solar cell based on dye-sensitized colloidal TiO_2 films. *Nature* **1991**, *353*, 737−740.

(2) Hagfeldt, A.; Grätzel, M. Light-induced redox reactions in nanocrystalline systems. *Chem. Rev.* **1995**, *95*, 49−68.

(3) Hagfeldt, A.; Grätzel, M. Molecular photovoltaics. *Acc. Chem. Res.* **2000**, *33*, 269−277.

(4) Grätzel, M. Photoelectrochemical cells. *Nature* **2001**, *414*, 338−344.

(5) Hagfeldt, A.; Boschloo, G.; Sun, L.; Kloo, L.; Pettersson, H. Dye-sensitized solar cells. *Chem. Rev.* **2010**, *110*, 6595−6663.

(6) Kallioinen, J.; Benkö, G.; Sundström, V.; Korppi-Tommola, J. E. I.; Yartsev, A. P. Electron transfer from the singlet and triplet excited states of $Ru(dcbpy)_2(NCS)_2$ into nanocrystalline TiO_2 thin films. *J. Phys. Chem. B* **2002**, *106*, 4396−4404.

(7) Kallioinen, J.; Benkö, G.; Myllyperkiö, P.; Khriachtchev, L.; Skårman, B.; Wallenberg, R.; Tuomikoski, M.; Korppi-Tommola, J. E. I.; Sundström, V.; Yartsev, A. P. Photoinduced ultrafast dynamics of $Ru(dcbpy)_2(NCS)_2$-sensitized nanocrystalline TiO_2 films: The influence of sample preparation and experimental conditions. *J. Phys. Chem. B* **2004**, *108*, 6365−6373.

(8) Myllyperkiö, P.; Benkö, G.; Korppi-Tommola, J. E. I.; Yartsev, A. P.; Sundström, V. A study of electron transfer in $Ru(dcbpy)_2(NCS)_2$ sensitized nanocrystalline TiO_2 and SnO_2 films induced by red-wing excitation. *Phys. Chem. Chem. Phys.* **2008**, *10*, 996−1002.

(9) Luitel, T.; Druffel, T.; Zamborini, F. P. Covalent modification of photoanodes for stable dye-sensitized solar cells. *Langmuir* **2013**. DOI: 10.1021/la402256v.

(10) Grünwald, R.; Tributsch, H. Mechanisms of instability in Ru-based dye sensitization solar cells. *J. Phys. Chem. B* **1997**, *101*, 2564−2575.

(11) Greijer Agrell, H.; Lindgren, J.; Hagfeldt, A. Degradation mechanisms in a dye-sensitized solar cell studied by UV-VIS and IR spectroscopy. *Sol. Energy* **2003**, *75*, 169−180.

(12) He, H.; Gurung, A.; Si, L. 8-Hydroxylquinoline as a strong alternative anchoring group for porphyrin-sensitized solar cells. *Chem. Commun.* **2012**, *48*, 5910−5912.

(13) Xue, G.; Guo, Y.; Yu, T.; Guan, J.; Yu, X.; Zhang, J.; Liu, J.; Zou, Z. Degradation mechanisms investigation for long-term thermal stability of dye-sensitized solar cells. *Int. J. Electrochem. Sci.* **2012**, *7*, 1496−1511.

(14) Lao, C.-F.; Chu, Z.-Z.; Zou, D.-C. Self-assembly of 3-aminopropyltrimethoxysilane to improve the efficiency of dye-sensitized solar cells. *Acta Phys. Chim. Sin.* **2011**, *27*, 419−424.

(15) Zhang, J.; Yang, G.; Sun, Q.; Zheng, J.; Wang, P.; Zhu, Y.; Zhao, X. The improved performance of dye sensitized solar cells by bifunctional aminosilane modified dye sensitized photoanode. *J. Renewable Sustainable Energy* **2010**, *2*, 013104.

(16) Quintana, M.; Edvinsson, T.; Hagfeldt, A.; Boschloo, G. Comparison of dye-sensitized ZnO and TiO_2 solar cells: Studies of charge transport and carrier lifetime. *J. Phys. Chem. C* **2007**, *111*, 1035−1041.

(17) Anderson, N. A.; Ai, X.; Lian, T. Q. Electron injection dynamics from Ru polypyridyl complexes to ZnO nanocrystalline thin films. *J. Phys. Chem. B* **2003**, *107*, 14414−14421.

(18) Bauer, C.; Boschloo, G.; Mukhtar, E.; Hagfeldt, A. Electron injection and recombination in $Ru(dcbpy)_2(NCS)_2$ sensitized nanostructured ZnO. *J. Phys. Chem. B* **2001**, *105*, 5585−5588.

(19) Katoh, R.; Furube, A.; Yoshihara, T.; Hara, K.; Fujihashi, G.; Takano, S.; Murata, S.; Arakawa, H.; Tachiya, M. Efficiencies of electron injection from excited N3 dye into nanocrystalline semiconductor (ZrO_2, TiO_2, ZnO, Nb_2O_5, SnO_2, In_2O_3) films. *J. Phys. Chem. B* **2004**, *108*, 4818−4822.

(20) Szarko, J. M.; Neubauer, A.; Bartelt, A.; Socaciu-Siebert, L.; Birkner, F.; Schwarzburg, K.; Hannappel, T.; Eichberger, R. The ultrafast temporal and spectral characterization of electron injection from perylene derivatives into ZnO and TiO_2 colloidal films. *J. Phys. Chem. C* **2008**, *112*, 10542−10552.

(21) Willis, R. L.; Olson, C.; O'Regan, B.; Lutz, T.; Nelson, J.; Durrant, J. R. Electron dynamics in nanocrystalline ZnO and TiO_2 films probed by potential step chronoamperometry and transient absorption spectroscopy. *J. Phys. Chem. B* **2002**, *106*, 7605−7613.

(22) Ramakrishna, G.; Ghosh, H. N.; Singh, A. K.; Palit, D. K.; Mittal, J. P. Dynamics of back-electron transfer processes of strongly coupled triphenyl methane dyes adsorbed on TiO_2 nanoparticle surface as studied by fast and ultrafast visible spectroscopy. *J. Phys. Chem. B* **2001**, *105*, 12786−12796.

(23) Argazzi, R.; Bignozzi, C. A.; Heimer, T. A.; Castellano, F. N.; Meyer, G. J. Long-lived photoinduced charge separation across nanocrystalline TiO_2 interfaces. *J. Am. Chem. Soc.* **1995**, *117*, 11815−11816.

(24) Kuciauskas, D.; Freund, M. S.; Gray, H. B.; Winkler, J. R.; Lewis, N. S. Electron transfer dynamics in nanocrystalline titanium dioxide solar cells sensitized with ruthenium or osmium polypyridyl complexes. *J. Phys. Chem. B* **2001**, *105*, 392−403.

(25) Pan, J.; Benkö, G.; Xu, Y. H.; Pascher, T.; Sun, L. C.; Sundström, V.; Polívka, T. Photoinduced electron transfer between a carotenoid and TiO_2 nanoparticle. *J. Am. Chem. Soc.* **2002**, *124*, 13949−13957.

(26) Asbury, J. B.; Hao, E. C.; Wang, Y. Q.; Lian, T. Q. Bridge length-dependent ultrafast electron transfer from Re polypyridyl complexes to nanocrystalline TiO_2 thin films studied by femtosecond infrared spectroscopy. *J. Phys. Chem. B* **2000**, *104*, 11957−11964.

(27) Marcus, R. A. On the theory of electron-transfer reactions. vi. unified treatment for homogeneous and electrode reactions. *J. Chem. Phys.* **1965**, *43*, 679−701.

(28) Gerischer, H. In *Physical Chemistry: an Advanced Treatise*; Eyring, H., Henderson, D., Jost, W., Eds.; Academic Press: New York, 1970; Vol. *IXA*, pp 463−542.

(29) Levich, V. G. In *Physical Chemistry, an Advanced Treatise*; Eyring, H., Henderson, D., Jost, W., Eds.; Academic Press: New York/London, 1970; Vol. *IXB*, Chapter 12, pp 985−1074.

(30) Anderson, N. A.; Ai, X.; Chen, D. T.; Mohler, D. L.; Lian, T. Q. Bridge-assisted ultrafast interfacial electron transfer to nanocrystalline SnO_2 thin films. *J. Phys. Chem. B* **2003**, *107*, 14231−14239.

(31) Bauer, C.; Teuscher, J.; Pelet, S.; Wenger, B.; Bonhôte, P.; Nazeeruddin, M. K.; Zakeeruddin, S. M.; Comte', P.; Grätzel, M.; Moser, J.-E. Ultrafast charge transfer through *p*-oligo(phenylene) bridges: effect of nonequilibrium vibrations. *Curr. Sci.* **2010**, *99*, 343−352.

(32) Bauer, C.; Teuscher, J.; Brauer, J. C.; Punzi, A.; Marchioro, A.; Ghadiri, E.; De Jonghe, J.; Wielopolski, M.; Banerji, N.; Moser, J.-E. Dynamics and mechanisms of interfacial photoinduced electron transfer processes of third generation photovoltaics and photocatalysis. *Chimia* **2011**, *65*, 704−709.

(33) Mieszawska, A. J.; Slawinski, G. W.; Zamborini, F. P. Directing the growth of highly aligned gold nanorods through a surface chemical amidation reaction. *J. Am. Chem. Soc.* **2006**, *128*, 5622−5623.
(34) Zeng, T.-W.; Liu, I.-S.; Huang, K.-T.; Liao, H.-C.; Chien, C.-T.; Wong, D. K.-P.; Chen, C.-W.; Wu, J.-J.; Chen, Y.-F.; Su, W.-F. Effects of bifunctional linker on the optical properties of ZnO nanocolumn-linker-CdSe quantum dots heterostructure. *J. Colloid Interface Sci.* **2011**, *358*, 323−328.
(35) Zhang, F.; Srinivasan, M. P. Self-assembled molecular films of aminosilanes and their immobilization capacities. *Langmuir* **2004**, *20*, 2309−2314.
(36) Fattori, A.; Peter, L. M.; Belding, S. R.; Compton, R. G.; Marken, F. Cis-bis(isothiocyanato)-bis(2,2′-bipyridyl-4,4′dicarboxylato)-Ru(II) (N719) dark-reactivity when bound to fluorine-doped tin oxide (FTO) or titanium dioxide (TiO_2) surfaces. *J. Electroanal. Chem.* **2010**, *640*, 61−67.
(37) Luitel, T.; Druffel, T.; Zamborini, F. P. Unpublished work.
(38) Wen, P.; Han, Y.; Zhao, W. Influence of TiO_2 nanocrystals fabricating dye-sensitized solar cell on the absorption spectra of N719 sensitizer. *Int. J. Photoenergy* **2012**, *2012*, 906198.
(39) Tachibana, Y.; Moser, J. E.; Grätzel, M.; Klug, D. R.; Durrant, J. R. Subpicosecond interfacial charge separation in dye-sensitized nanocrystalline titanium dioxide films. *J. Phys. Chem.* **1996**, *100*, 20056−20062.
(40) Liang, Y.; Peng, B.; Chen, J. Correlating dye adsorption behavior with the open-circuit voltage of triphenylamine-based dye-sensitized solar cells. *J. Phys. Chem. C* **2010**, *114*, 10992−10998.
(41) Dell'Orto, E.; Raimondo, L.; Sassella, A.; Abbotto, A. Dye-sensitized solar cells: Spectroscopic evaluation of dye loading on TiO_2. *J. Mater. Chem.* **2012**, *22*, 11364−11369.
(42) Nazeeruddin, M. K.; Humphry-Baker, R.; Liska, P.; Grätzel, M. Investigation of sensitizer adsorption and the influence of protons on current and voltage of a dye-sensitized nanocrystalline TiO_2 solar cell. *J. Phys. Chem. B* **2003**, *107*, 8981−8987.
(43) Benkö, G.; Kallioinen, J.; Korppi-Tommola, J. E. I.; Yartsev, A. P.; Sundström, V. Photoinduced ultrafast dye-to-semiconductor electron injection from nonthermalized and thermalized donor states. *J. Am. Chem. Soc.* **2002**, *124*, 489−493.
(44) Benkö, G.; Kallioinen, J.; Myllyperkiö, P.; Trif, F.; Korppi-Tommola, J. E. I.; Yartsev, A. P.; Sundström, V. Interligand electron transfer determines triplet excited state electron injection in RuN3-sensitized TiO_2 films. *J. Phys. Chem. B* **2004**, *108*, 2862−2867.
(45) Bräm, O.; Cannizzo, A.; Chergui, M. Ultrafast fluorescence studies of dye sensitized solar cells. *Phys. Chem. Chem. Phys.* **2012**, *14*, 7934−7937.
(46) Wenger, B.; Grätzel, M.; Moser, J.-E. Rationale for kinetic heterogeneity of ultrafast light-induced electron transfer from Ru(II) complex sensitizers to nanocrystalline TiO_2. *J. Am. Chem. Soc.* **2005**, *127*, 12150−12151.
(47) Huber, R.; Spörlein, S.; Moser, J. E.; Grätzel, M.; Wachtveitl, J. The role of surface states in the ultrafast photoinduced electron transfer from sensitizing dye molecules to semiconductor colloids. *J. Phys. Chem. B* **2000**, *104*, 8995−9003.
(48) Valeur, B. *Molecular Fluorescence: Principles and Applications*; Wiley: Wineheim, 2001.
(49) Moser, J.-E. In *Dye-sensitized solar cells*; Kalyanasundaram, K., Ed.; CRC: Lausanne, 2010; Chapter 11, pp 401−456.
(50) Smeigh, A. L.; Katz, J. E.; Brunschwig, B. S.; Lewis, N. S.; McCusker, J. K. Effect of the presence of iodide on the electron injection dynamics of dye-sensitized TiO_2-based solar cells. *J. Phys. Chem. C* **2008**, *112*, 12065−12068.
(51) Bauer, C.; Boschloo, G.; Mukhtar, E.; Hagfeldt, A. Ultrafast studies of electron injection in Ru dye sensitized SnO_2 nanocrystalline thin film. *Int. J. Photoenergy* **2002**, *4*, 17−20.
(52) Huang, J.; Stockwell, D.; Boulesbaa, A.; Guo, J.; Lian, T. Comparison of electron injection dynamics from rhodamine B to In_2O_3, SnO_2, and ZnO nanocrystalline thin films. *J. Phys. Chem. C* **2008**, *112*, 5203−5212.